JMEPEG (2005) 14:388-394
DOI: 10.1361/10599490523931


1059-9495/$19.00

# Finite-Element Analysis on Thermomechanical Behavior of a Marine Propeller Casting in the Sand-Casting Process

*Sung-Mo Lee and Won-Jae Lee*

*(Submitted November 21, 2004; in revised form April 5, 2005)*

**Thermal deformation of a large marine propeller casting during solidification and cooling was analyzed by a coupled thermomechanical finite-element analysis (FEA). The calculated displacements on the blade in the *z*-direction were compared with the measured values that confirmed the effectiveness of FEA for the prediction of thermal deformation. The effect of the shake-out time and method on the deformation of the propeller casting was also investigated. The longer the shake-out time, the smaller the deformation. For controlling the deformation of the propeller casting, the sequential shake-out was a more efficient method than the simultaneous shake-out.**

**Keywords** finite-element method, marine propeller, numerical analysis, sand casting, thermal deformation

## 1. Introduction

A large marine propeller is generally manufactured by a sand casting. The pouring weight ranges from 20 to 120 tons, depending on the propeller type. The blades of the propeller are deformed during solidification and cooling due to the thermal stresses generated by the difference in local cooling rate. The casting dimension has been designed by experience in considering the deformation of blades. Due to this, it is difficult to design the optimal dimension for a new type of propeller casting.

Finite-element analysis (FEA) can be applied to predict the deformation in the propeller casting. The FEA of thermal stress during solidification is of considerable significance in predicting casting deformation (Ref 1-7). The deformation of casting during solidification is very complicated due to the complex mechanical behavior of the liquid zone, the liquid-solid coexistence zone, and the solid zone at high temperature (Ref 8, 9). Thus, it is necessary to establish the numerical analysis method to predict the casting deformation both to eliminate unnecessary trial and error and to optimize the machining work.

In this study, the effect of the shake-out time and method on the deformation of the propeller casting has been investigated using a commercial code ProCAST, which provides a coupled thermoelastoplastic model (Ref 10). The results of FEA were compared with those of the measurement to validate the numerical analysis method.

**Sung-Mo Lee** and **Won-Jae Lee,** Material Research Department, Hyundai Industrial Research Institute, Hyundai Heavy Industries Co. Ltd., 1 Cheonha-dong, Dong-gu, Ulsan, Republic of Korea, 682-792. Contact e-mail: leesm12@hhi.co.kr.

## 2. Experimental Procedure

An experiment of block casting was performed to set up the simulation condition. A Ni-Al bronze-casting block with the chemical compositions given in Table 1 was made by a sand-casting process. The inner surface of the mold was coated with coating ingredients (gracote) to make the ease of separation of the solidified casting block from the mold. The mold was sufficiently dried at 250 °C just before the melts were poured into it. All of the melts were made by melting virgin Ni-Al bronze ingots. Nitrogen gas was purged into a Ni-Al bronze melt to eliminate hydrogen gas-inducing casting defects such as porosity in the casting block. The pouring temperature was 1135 °C. The top part of the casting block was covered with exothermic powder (60%$SiO_2$-17%metal Al-7%$Fe_2O_3$) just after casting to protect the rapid solidification of the melt acting as an open riser. The dimensions of the casting block and the position of the thermocouple are shown in Fig. 1. The experimental procedure is shown in Fig. 2. The K-type thermocouple and data recorder were used to plot the cooling curve (Ref 11, 12). The height from the ground to the lower surface of the blade was measured after cooling down to room temperature. Deformation can be evaluated by comparing the measured

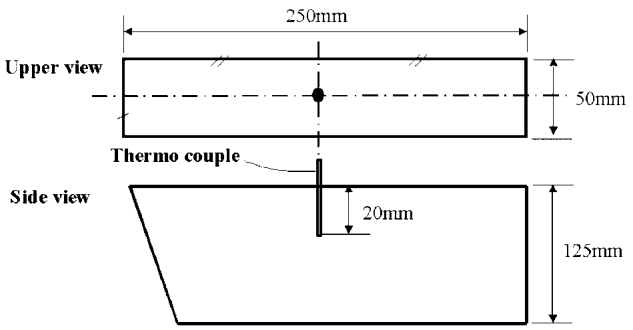


**Fig. 1** The dimensions of the casting block and the position of the thermocouple

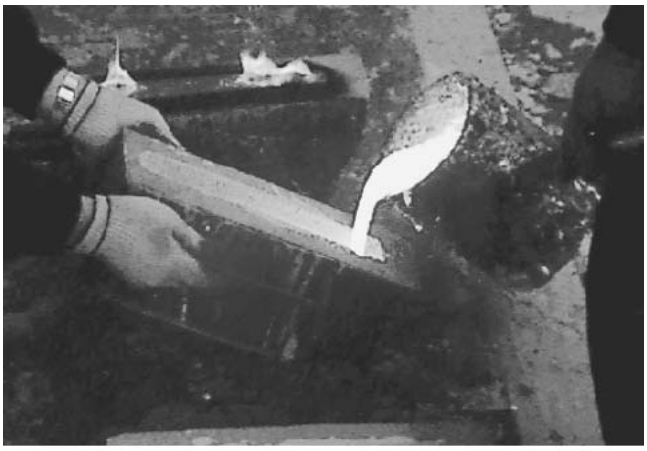

(a)

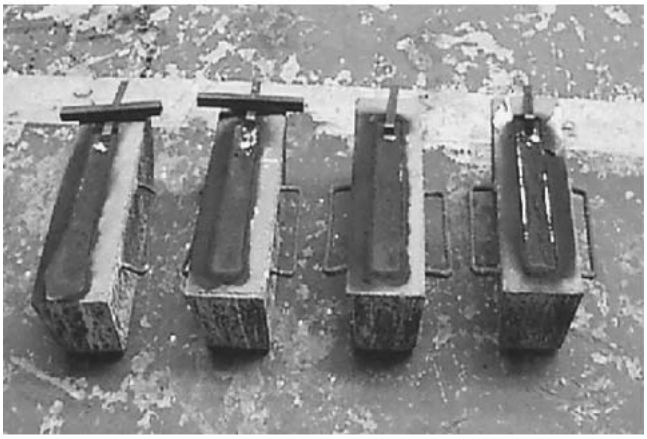

(b)

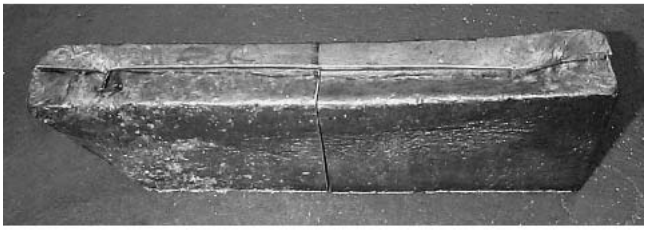

(c)

**Fig. 2** Experimental procedure: (a) during pouring; (b) casting block after being covered with exothermic powder; and (c) the casting block after shake-out

**Table 1 Chemical composition of Ni-Al bronze casting employed in the experiment (in weight percent)**

| Cu | Al | Ni | Fe | Mn | Zn | Sn | Pb | Si | P |
|---|---|---|---|---|---|---|---|---|---|
| 79.6~ 79.8 | 9.70~ 9.75 | 4.80~ 4.83 | 4.54~ 4.68 | 0.91~ 0.92 | 0.10 | 0.03 | 0.02 | 0.06~ 0.07 | 0.020~ 0.021 |

height with the dimensions of the wood pattern. The measurement was performed at 12 points, as shown in Fig. 3. The propeller casting after the riser and the gating system were removed is shown in Fig. 4. The pouring weight was 21 tons.

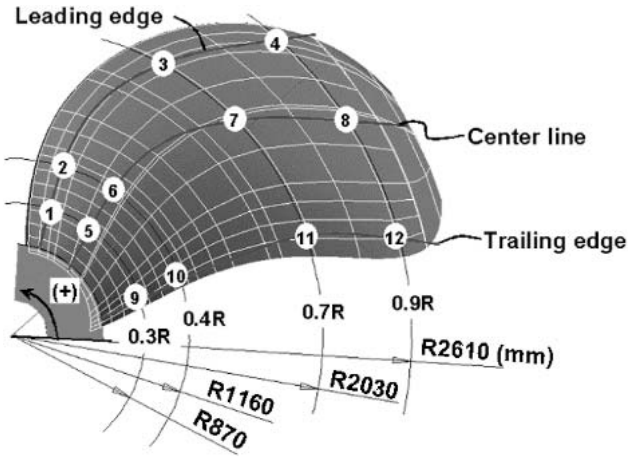


**Fig. 3** Positions for the deformation measurements

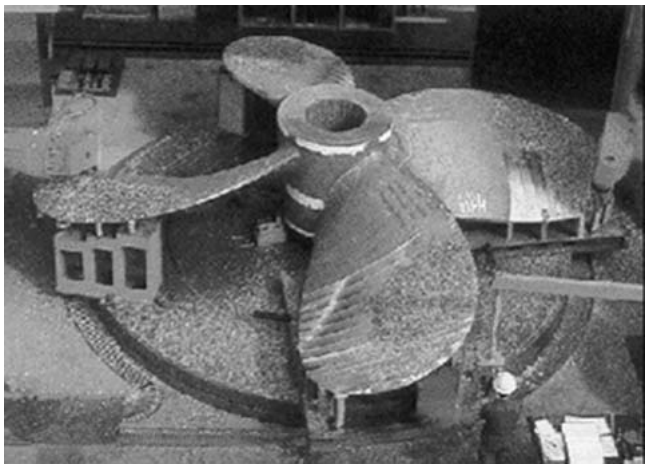

**Fig. 4** Propeller casting after the riser and the gating system were removed

## 3. Finite-Element Analysis

A three-dimensional computer-aided design (CAD) model and FEA model of the propeller and mold (one-quarter model) were created, consisting of 180,000 tetrahedral elements, as shown in Fig. 5 and 6, respectively. The diameter of the propeller was 5,800 mm. A rotational symmetric boundary condition was applied to the symmetric faces. It was assumed that the surface of the riser was adiabatic, because the amount of heat generation by exothermic powder on the surface of the riser was not high in the actual casting. The FEA was performed using a coupled thermoelastoplastic model. The initial temperatures of casting and of the inner and outer sleeves were assigned to 1135 and 130 °C, respectively, based on the casting condition in the foundry shop. The physical and mechanical properties used in the FEA are listed in Table 2. A thermoelastoplastic model was used for the casting. The heat-transfer coefficients were determined by an experiment of block casting to consider the interface conditions between the mold and the casting. The shake-out time and method investigated are summarized in Table 3. The shake-out times were 18, 54, and 74 h. The conditions of the shake-out method were the sequential

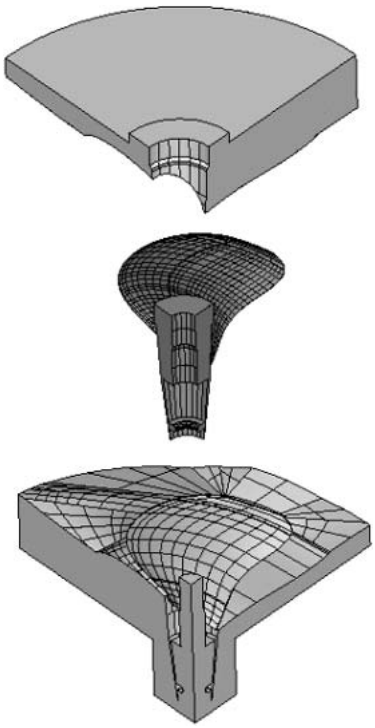

**Fig. 5** The CAD model of the casting and the mold (one-quarter model)

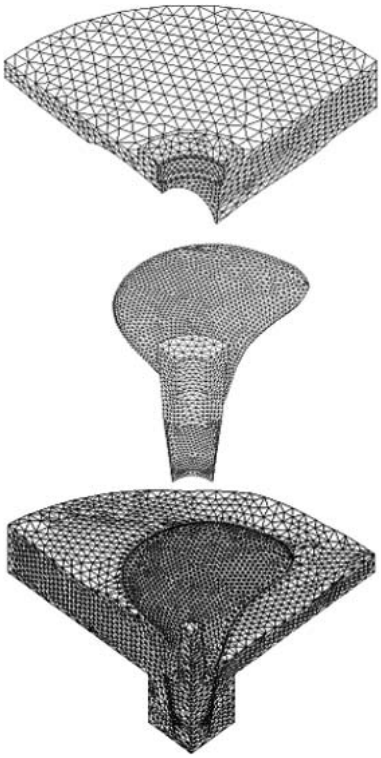

**Fig. 6** The FEA model of the casting and the mold (one-quarter model)

shake-out and the simultaneous shake-out. The sequential shake-out involves removing the lower mold after removing the upper mold. The simultaneous shake-out condition involves the removal of the upper and lower molds simultaneously.

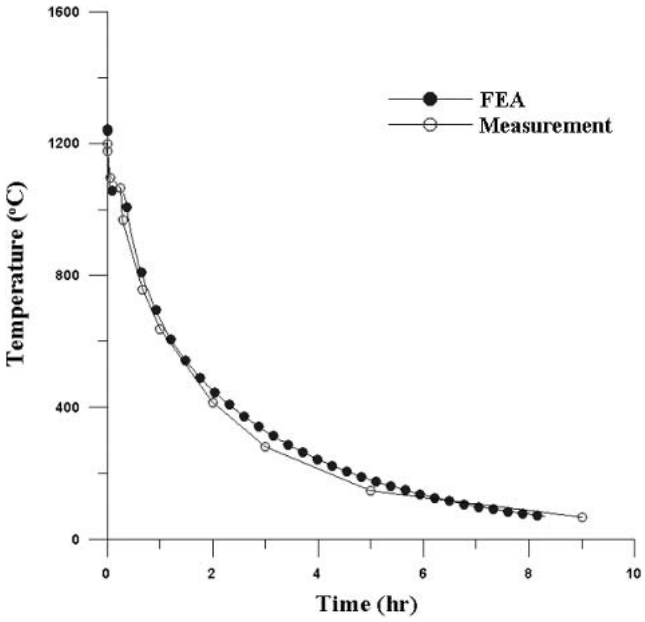


**Fig. 7** Comparison of the calculated and measured cooling curves at the block casting

**Table 2 Material properties used in finite-element analysis**

| Properties | Unit | Casting | Mold | Sleeve |
|---|---|---|---|---|
| Material | … | Ni-Al bronze | Silica sand | Insulator |
| Conductivity(a) | W/m · K | 51 ~ 80 | 0.733 ~ 0.59 | 0.06 ~ 0.13 |
| Density | kg/m$^3$ | 7600 ~ 6000* | 1520 | 500 |
| Specific heat(a) | kJ/kg · K | 0.42 ~ 5.74 | 0.676 ~ 1.23 | 0.4 ~ 0.74 |
| Stress model | … | Elasto-plastic | Rigid | Rigid |
| Elastic modulus(a) | GPa | 127 ~ 10 | … | … |
| Poisson's ratio | … | 0.32 | … | … |
| Thermal expansion coefficient(a) | $10^{-5}$/°C | 1.64 ~ 2.17 | … | … |
| Yield stress(a) | MPa | 260 ~ 5 | … | … |
| Plastic Modulus | MPa | 8250 | … | … |

(a) The properties are a function of the temperature.

**Table 3 Shake-out time and method**

| Shake-out method | | Shake-out time, h | | |
|---|---|---|---|---|
| Sequential shake-out | Upper mold | 14 | 34 | 44 |
| | Lower mold | 18 | 54 | 74 |
| Simultaneous shake-out | Upper and lower mold | 18 | 54 | 74 |

The rate representation of the total strain in the elastoplastic model (Ref 13) is given in Eq 1:

$$\dot{\varepsilon} = \dot{\varepsilon}^{e} + \dot{\varepsilon}^{p} + \dot{\varepsilon}^{T} \quad \text{(Eq 1)}$$

The linear isotropic elastic response is given in Eq 2:

$$\dot{\sigma} = E : (\dot{\varepsilon} - \dot{\varepsilon}^{p} - \dot{\varepsilon}^{T}) \quad \text{(Eq 2)}$$

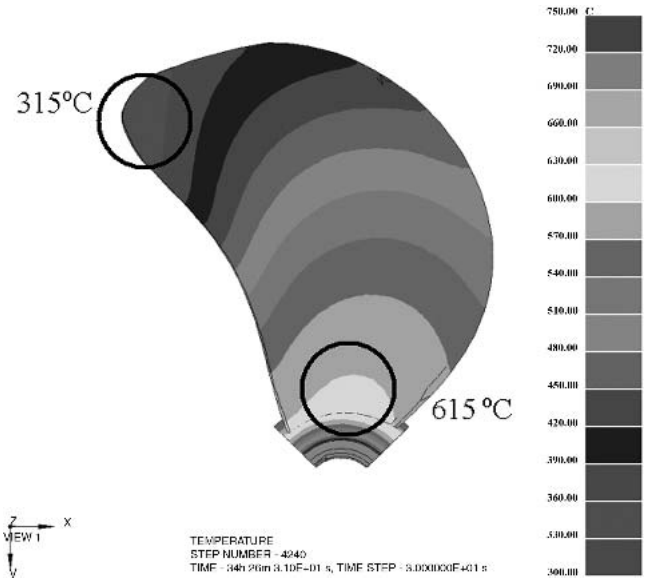


**Fig. 8** Distribution of the temperature on the lower surface of the propeller casting (sequential shake-out with shake-out times of 54 and 34.5 h after pouring)

**Table 4 Heat transfer coefficients used in finite-element analysis**

| Interface | Heat transfer coefficient, (cal/cm$^2$ per s/°C) |
|---|---|
| Cast/mold | 0.003 |
| Cast/sleeve | $10^{-9} \sim 0.003$ |
| Sleeve/mold | $10^{-9}$ |
| Mold/mold | 0.00005 |

where $E$ is the elastic constitutive tensor, $\dot{\varepsilon}^{e}$ is the elastic strain rate, $\dot{\varepsilon}^{p}$ is the plastic strain rate, and $\dot{\varepsilon}^{T}$ is the thermal strain rate.

A von Mises yield function used in the numerical computations is given in Eq 3:

$$f = \sqrt{\frac{3}{2}}\|\mathbf{s}\| - \kappa \qquad \text{(Eq 3)}$$

$\mathbf{s} = \boldsymbol{\sigma} - \frac{1}{3}(tr\boldsymbol{\sigma})\,\mathbf{I}$: deviatoric stresses, $\kappa$: characterized isotropic hardining.

The assumed plastic flow rule has the form of $\dot{\varepsilon}^{p} = \gamma\,(\partial f/\partial\boldsymbol{\sigma})$, where $\gamma$ is the plastic multiplier to be determined with the aid of the consistency condition, $f = 0$.

Linear isotropic hardening is given in Eq 4:

$$\kappa = Y_0 + H\bar{\varepsilon}^{p} \qquad \text{(Eq 4)}$$

where $Y_0$: yield stress, H: plastic modulus, effective plastic strain:

$$\bar{\varepsilon}^{p} = \int_0^t \sqrt{\frac{2}{3}\,\dot{\varepsilon}^{p} : \dot{\varepsilon}^{p}}\,d\tau$$

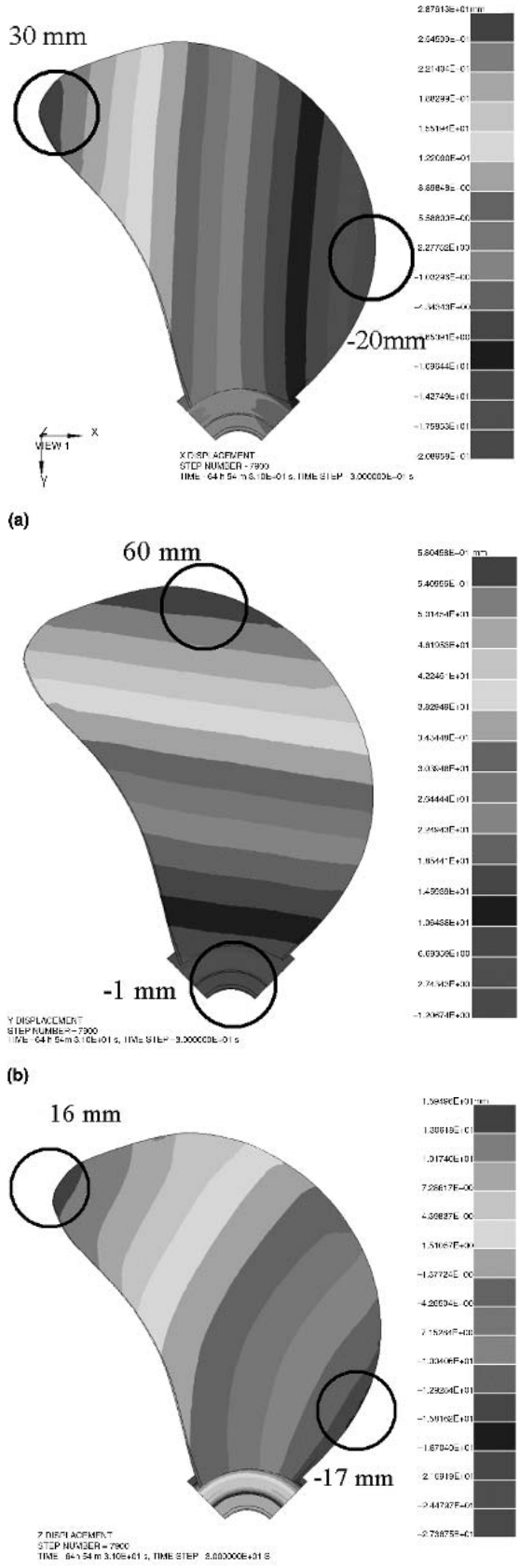


**Fig. 9** The distribution of the displacement during solidification on the lower surface of the propeller casting (sequential shake-out with shake-out time of 54 h, with an additional cooling time of 11 h): (a) $x$-direction; (b) $y$-direction; (c) $z$-direction

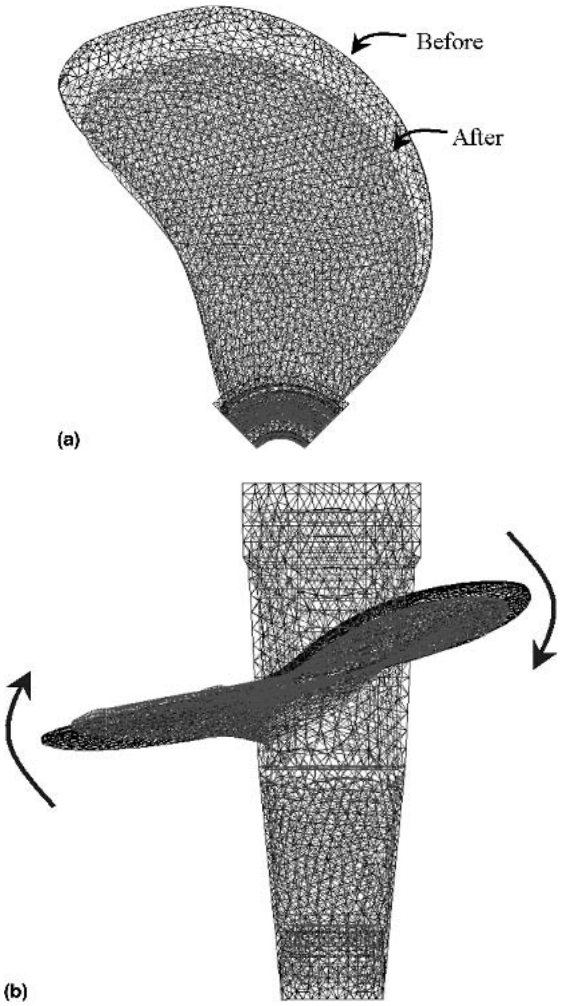


**Fig. 10** Comparison of the propeller shape before and after deformation (sequential shake-out time of 54 h, with an additional cooling time of 11 h; magnification ×5): (a) lower view; (b) side view

The isotropic hardening rule can alternatively have the saturation form of Eq 5:

$$\kappa = Y_\infty + (Y_0 - Y_\infty)e^{-\alpha\bar{\varepsilon}^p} \quad \text{(Eq 5)}$$

$Y_\infty$: ultimate stress, $\alpha$: material parameter.

One of the critical aspects of the calculation is the treatment of the interfaces between the casting and mold, considering both the thermal and mechanical aspects. A multibody mechanical contact algorithm is used to compute the contact and gap formation between the casting and mold parts. Contact between different mold parts is also considered. An augmented Lagrangian-type method (Ref 14) is used in the contact algorithm. An additional automatic penalty number adjustment technique is implemented in the algorithm. Such a technique greatly enhances the stability and robustness of the contact computation algorithm. The variational form of the equilibrium equation with mechanical contact at any time $t$ is written as Eq 6. A frictionless contact is considered for simplicity:

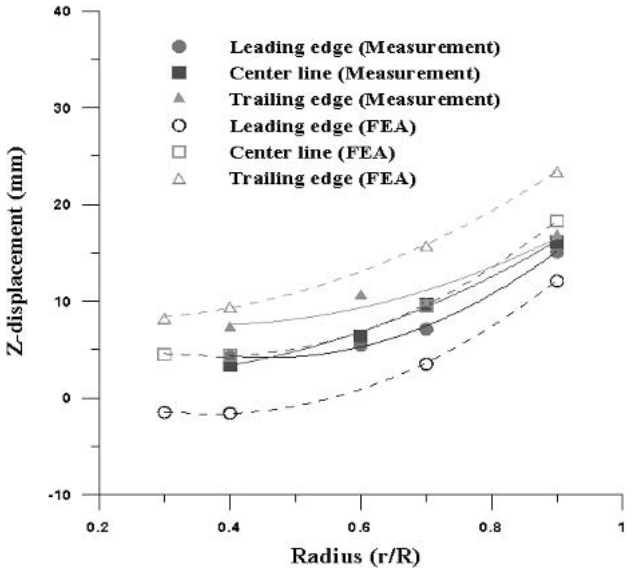


**Fig. 11** Comparison of the calculated and measured displacements in the $z$-direction

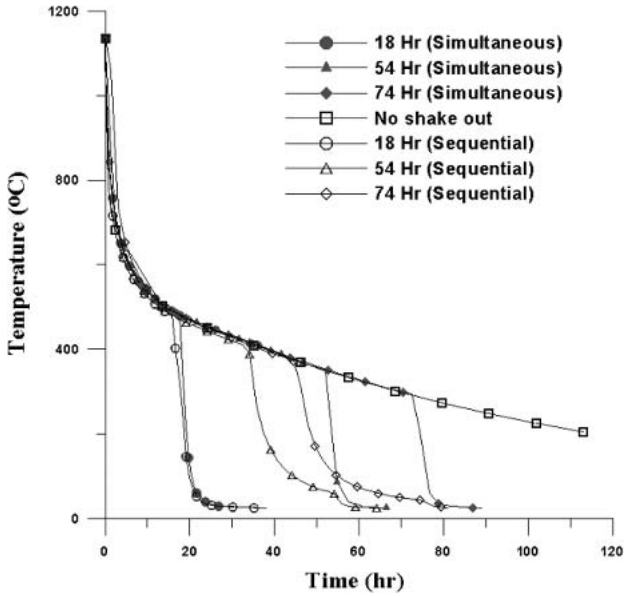


**Fig. 12** Calculated cooling curves of the propeller casting at point 12 on the 0.9R trailing edge of the blade

$$\int_\Omega \sigma \cdot grad(\delta\mathbf{u})d\Omega - \int_\Omega \mathbf{b} \cdot \delta\mathbf{u}d\Omega - \int_{\Gamma_\sigma} \bar{\mathbf{t}} \cdot \delta\mathbf{u}d\Gamma + \int_{\Gamma_c} \langle \lambda^k + \xi g(\mathbf{u}) \rangle \mathbf{n} \cdot \delta\mathbf{u}d\Gamma = 0 \quad \text{(Eq 6)}$$

where $\Omega$ is the geometry of the casting and all the die parts, $\Gamma$ is all of the contact interface between all parts, $t$: surface tractions, $\langle \lambda^k + \xi g(\mathbf{u}) \rangle$: augmented Lagrangian multiplier, $\xi$: penalty number b: body forces:

Thermal contact between parts is considered by adjusting the interface heat-transfer coefficient with respect to either the air-gap width or the contact pressure as computed by the mechanical contact algorithm. When the gap width is greater than

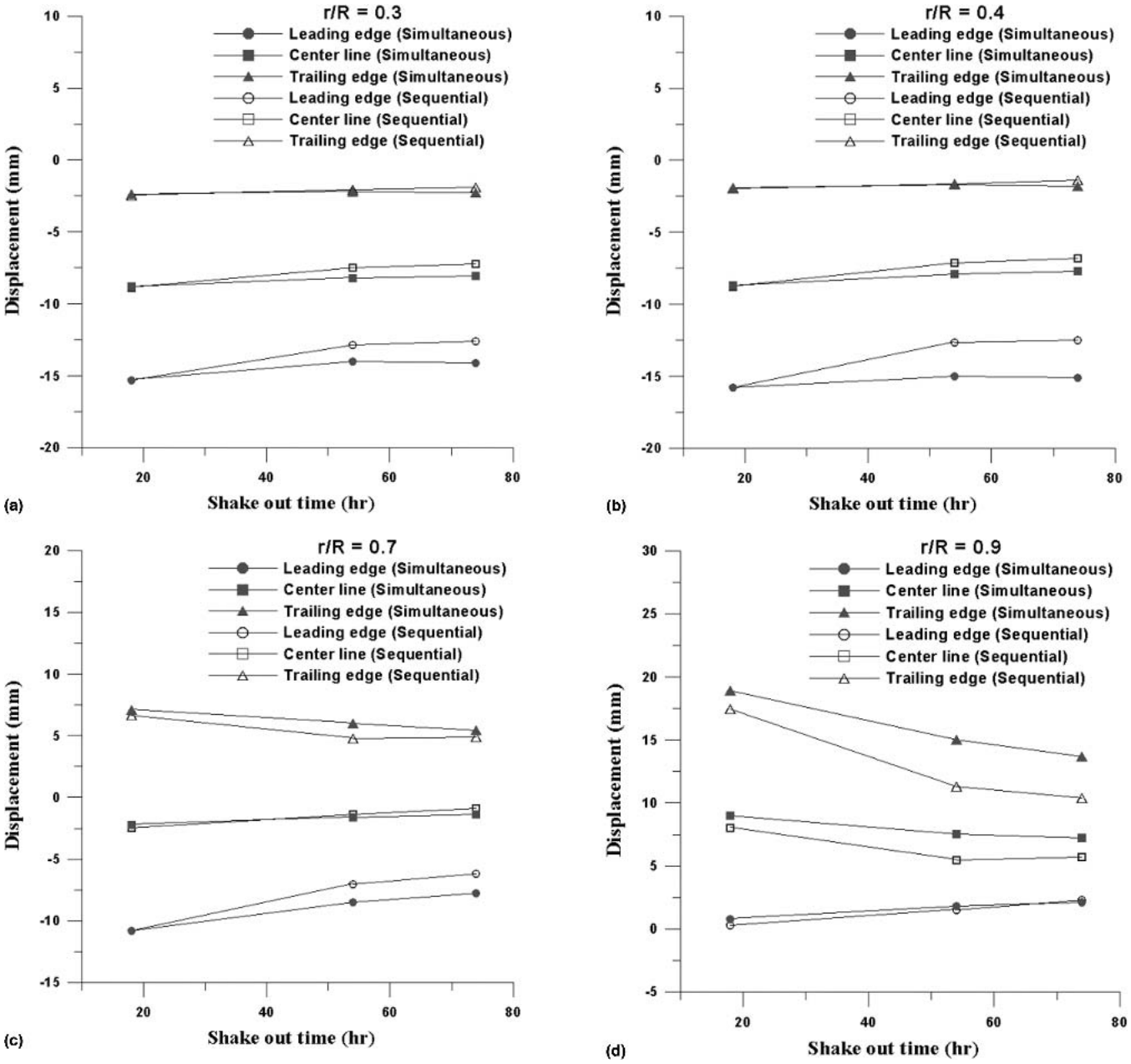


**Fig. 13** Effects of the shake-out time and method on the displacement in the *z*-direction: (a) 0.3R; (b) 0.4R; (c) 0.7R; and (d) 0.9R

zero, the adjusted heat-transfer coefficient has the form given in Eq 7:

$$h_{\text{eff}} = \frac{1}{\frac{1}{h_0} + \frac{1}{(h_{\text{air}} + h_{\text{rad}})}} \qquad \text{(Eq 7)}$$

$h_0$: initial value of the heat transfer coefficient, $h_{\text{air}}$: $k_{\text{air}}/g$, $g$: gap width, $h_{\text{rad}}$: radiation heat transfer coefficient $k_{\text{air}}$: conductivity of air or 0 for vacuum.

If the contact pressure is greater than zero, the effective heat transfer increases linearly with the pressure up to a maximum value. When the casting is ejected from the die, the mechanical contact is no longer applied to the casting-die interfaces. Care must then be taken to apply an appropriate displacement constraint to prevent solid-body movement (Ref 10).

## 4. Results and Discussion

An experiment of block casting was performed to determine the heat-transfer coefficients. The calculated and measured cooling curves are in good agreement, as shown in Fig. 7. The heat-transfer coefficients used in the FEA are summarized in Table 4.

The FEA was performed to predict the thermomechanical behavior of the propeller casting. Figure 8 shows the distribution of the temperature on the lower surface of the propeller casting for the sequential shake-out time of 54 h, when 34.5 h passed after pouring. The temperatures on the thin tip of the blade and at the thick intersection of the boss and the blade were 315 and 615 °C, respectively. The nonuniform temperature distribution due to the difference of casting thickness should result in thermal deformation. Figure 9 shows the dis-

tribution of the displacement on the lower surface of the propeller casting for the sequential shake-out time of 54 h. The displacement in the *x*-direction was ~30 mm on the tip of the blade and –20 mm on the leading edge, as shown in Fig. 9(a). The displacement in the *y*-direction was ~60 mm on the tip of the blade and −1 mm at the boss, as shown in Fig. 9(b). The displacement in the *z*-direction was ~16 mm on the tip of the blade and –17 mm on the leading edge near to the boss, as shown in Fig. 9(c). The propeller shapes before and after deformation were compared, as shown in Fig. 10. Figure 9(a) and (b) and Fig. 10(a) show that the contraction is developed toward the centerline of the blade and the boss. The positive displacement on the thin tip of the blade and the negative displacement on the thick leading edge in the *z*-direction were developed, as shown in Fig. 9(c) and 10(b). The displacements in the *z*-direction on the tip of blade and on the thin trailing edge were larger than that in the *z*-direction near the boss and on the thick leading edge. That is why the negative contraction offsets the positive displacement near the boss and on the thick leading edge. Thus, the deformation of propeller casting consists of contraction in the *x*- and *y*-direction, and distortion in the *z*-direction.

The calculated displacements on the blade in the *z*-direction were compared with the measured values to validate the effectiveness of FEA for the prediction of thermal deformation. The calculated and measured displacements in the *z*-direction are compared in Fig. 11. They are in good agreement with a similar trend that the displacement increases with an increase in *r*/*R*. The base surface of the calculated value is the bottom of a whole casting, but that of the measured value is the bottom of the casting after cutting the skirt and gate systems.

The FEA was performed to evaluate the effect of the shake-out time and method on the cooling rate of the propeller casting. The calculated cooling curves of the propeller casting at point 12, where the largest deformation was developed, are shown in Fig. 12. The temperature of the propeller casting rapidly decreases just after shake-out. In the case of a simultaneous shake-out, the cooling rate was much higher than that for the sequential shake-out.

The effect of the shake-out time and method on the deformation of the propeller casting was also investigated by FEA. The results obtained from FEA are shown in the Fig. 13. The longer the shake-out time, the smaller the displacement in the *z*-direction. For the sequential shake-out, the displacements in the *z*-direction on the 0.9R trailing edge were 17.4 mm for a shake-out time of 18 h, 11.3 mm for a shake-out time of 54 h, and 10.4 mm for a shake-out time of 74 h. The differences in the displacements between shake-out times of 18 and 54 h, and between shake-out times of 54 and 74 h were 6.1 and 0.9 mm, respectively. A close look at Fig. 13 shows that the results for a shake-out time of 54 h are very close to those for a shake-out time of 74 h. This means that the shake-out time of 54 h is appropriate considering the working efficiency. The displacement in the *z*-direction for the simultaneous shake-out was much larger than that for the sequential shake-out. For the deformation control of the propeller casting, the sequential shake-out was a more efficient method than the simultaneous shake-out. The appropriate shake-out conditions obtained from FEA agreed with those obtained from trial and error. It was possible to determine the appropriate shake-out time and method using FEA in the manufacture of the new type of propeller casting.

## 5. Conclusions

The main conclusions obtained are summarized as follows.

- A three-dimensional numerical analysis method to predict the deformation of the propeller casting during solidification and cooling was established.
- The longer the shake-out time, the smaller the deformation.
- The deformation of the sequential shake-out was smaller than that of simultaneous shake-out.

### References


1. D. M. Lipinski, W. Schaefer, and S. Andersen, Numerical Modeling of the Filling Sequence, Solidification and Thermal Stresses of Castings, *Proceedings of the International Association for Mathematics and Computers in Simulation,* Berlin, 1997
2. D. Metzger, K. Jarrett New, and J. Dantzig, A Sand Surface Element for Efficient Modeling of Residual Stress in Castings, *Appl. Math. Modell.,* Vol 25, 2001, p 825-842
3. O.K. Kim, B.K. Koo, and S.H. Min, Analysis on the Elasto-Plastic Thermal Stress and Deformation of Metal Casting Mould by FEM (Finite Element Method), *J. Korean Foundrymen's Soc.,* Vol 13 (No. 1), 1991, p 81-93
4. S.H. Lee, H.N. Han, D.N. Lee, K.H. Oh, J.K. Park, J. Choi, and C.H. Yim, Finite Element Analysis of Mold Deformation during Continuous Casting, *J. Korean Inst. Met. Mater.,* Vol 35 (No. 1), 1997, p 87-95
5. Y. Song, Y. Yan, R. Zhang, Q. Lu, and D. Xu, Three Dimensional Non-Linear Coupled Thermo-Mechanical FEM Analysis of the Dimensional Accuracy for Casting Dies in Rapid Tooling, *Finite Elements Analysis Design,* Vol 38, 2001, p 79-91
6. D.J. Celentano, A Large Strain Thermoviscoplastic Formulation for the Solidification of S.G. Cast Iron in a Green Sand Mould, *Int. J. Plasticity,* Vol 17, 2001, p 1623-1658
7. S. Sen, B. Aksakal, and A. Ozel, Transient and Residual Thermal Stresses in Quenched Cylindrical Bodies, *Int. J. Mech. Sci.,* Vol 42, 2000, p 2013-2029
8. Liu, Kang, and Xiong, A Study on the Numerical Simulation of Thermal Stress during the Solidification of Shaped Castings, *Sci. Technol. Adv. Mater.,* Vol 2, 2001, p 157-164
9. J. Campbell, *Castings,* 2nd ed., Butterworth-Heinemann, 2003, p 259-266
10. UES Software, Inc., *User's Manual & Technical Reference,* UES Software, Inc., 2000
11. T.D. Park, D.Y. Kim, and J.G. Youn, "A Study on Factors Determining Tensile Properties of Ni-Al-Bronze Casting," AFS 105th Casting Congress: Copper Alloy Division (Dallas, TX), American Foundrymen's Society, 2001, p 3-8
12. T.D. Park, S.M. Lee, K.H. Kim, W.J. Lee, and J.K. Chun, "A Study on the Improvement of Mechanical Properties of Ni-Al Bronze Casting," Autumn Meeting of the Korean Foundrymen's Society (Jin-Ju, Korea), 2003
13. J.C. Simo and T.J.R. Hughes, Computational Inelasticity, Springer, 1998
14. J.C. Simo and T.A. Laursen, An Augmented Lagrangian Treatment of Contact Problems Involving Friction, *Comput. Struct.,* Vol 42, 1992, p 97-116